What controls the growth of the Himalayan foreland fold-and-thrust belt?

John Hirschmiller[1], Djordje Grujic[1], Bodo Bookhagen[2], Isabelle Coutand[1], Pascale Huyghe[3], Jean-Louis Mugnier[3], and Tank Ojha[4]

[1]Department of Earth Sciences, Dalhousie University, Halifax, Nova Scotia B3H 4R2, Canada
[2]Geography Department, University of California–Santa Barbara, Santa Barbara, California 93106-4060, USA
[3]Centre National de la Recherche Scientifique, Université J. Fourier, Maison des Géosciences BP 53, 38041 Grenoble Cedex, France
[4]Department of Geosciences, University of Arizona, Tucson, Arizona 85721, USA

ABSTRACT

We provide empirical evidence for the impact of surface processes on the structure of the present-day foreland fold-and-thrust belt of the Himalaya. We have reconstructed and analyzed ten balanced cross sections distributed along the entire length of the Himalayan arc. Here, we focus on the Siwalik Group, which represents the deformed part of the foreland basin and consists of synorogenic Middle Miocene to Pleistocene sediments that form the youngest and frontal part of the Himalayan orogen. We make two important observations: (1) a distinct west-to-east increase in strain and strain rate correlates with plate convergence rates, and (2) belt morphology is inversely correlated with rainfall amount. According to the predictions of the critical taper model, an eastward increase in convergence rate would induce higher rates of material accretion. Thus, the Himalayan fold-and-thrust belt should widen eastward, yet we have observed the opposite. However, higher annual rainfall amounts and specific stream power appear to favor a narrower belt. Thus, we suggest that the morphology of the Himalayan foreland fold-and-thrust belt is controlled primarily by surface processes, in accordance with the critical taper model.

INTRODUCTION

Interactions and feedbacks between tectonics and surface processes are affecting crustal deformation (Beaumont et al., 1992; Willett et al., 1993; Whipple, 2009). Although sophisticated numerical models can simulate the details of such interactions, unambiguous field evidence remains scarce.

Upper crustal deformation can be observed directly in active orogens, and the parameters controlling the deformation and morphology of critical Coulomb wedges have been well established. Here, we investigate the present-day foreland fold-and-thrust belt (FTB) of the Himalayan orogen (Avouac, 2003). Dahlen (1990) defined the steady-state width of a uniformly eroding wedge as $\dot{e}W\sec(\alpha + \beta) \approx \dot{e}W = hV$, where $\dot{e}$ is erosion rate, W is wedge width, h is the thickness of incoming sediments, and V is the velocity of convergence, and α and β are the surface slope and dip of the basal décollement, respectively. Such morphological elements and growth parameters can be constrained precisely in the Himalayan FTB.

Previous studies of the Himalayan FTB have either concentrated on narrow segments (e.g., Mugnier et al., 1999) or assumed that the critical Coulomb wedge extends from the frontal thrust to the suture zone and exhibits constant morphology along the entire orogenic arc (e.g., Hilley and Strecker, 2004). However, convergence rates between India and Eurasia (Molnar and Stock, 2009) and precipitation over the Himalaya (Bookhagen and Burbank, 2010) decrease significantly from east to west. This suggests the possibility of systematic variations in the morphology and growth rate of the Himalayan FTB and raises questions regarding the dominant factors forcing these variations. To address these questions, we constructed balanced cross sections covering the entire Himalayan arc, calculated shortening amounts and rates, and constrained climatic gradients linked to surface erosion.

GEOLOGICAL SETTING

From south to north, the primary structures extending along the Himalayan orogen (Fig. 1) are the Main Frontal thrust (MFT), Main Boundary thrust (MBT), Main Central thrust, and South Tibetan detachment (Hodges, 2000). Although published opinions vary, we contend that the active Himalayan FTB is delineated by the MFT (frontal thrust) and MBT (backstop), with foreland sediments (molasse) deformed in the style of fold-and-thrust belts lying between the two. The molasse consists of Middle Miocene to Pleistocene alluvial sandstones, mudstones, siltstones, and conglomerates and is divided lithostratigraphically into the Lower, Middle, and Upper Siwalik subgroups (Burbank et al., 1996).

Based on growth strata in central Nepal, Mugnier et al. (2004) inferred the onset of thrusting on the MFT to have occurred at ca. 2.4–1.8 Ma.

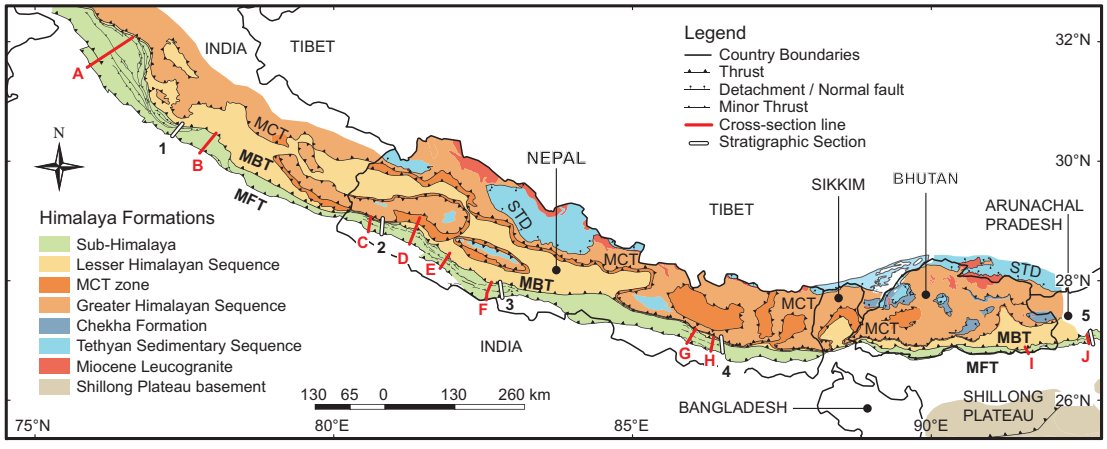

Figure 1. Geological overview map of the Himalaya with section locations. Balanced cross sections of Siwalik Group are indicated with red lines labeled A–J and are listed in Table 1. White lines 1–5 indicate detailed stratigraphic section locations with magnetostratigraphy (Fig. DR1 [see footnote 1]); MBT—Main Boundary thrust; MCT—Main Central thrust; MFT—Main Frontal thrust; STD—South Tibetan detachment. Map compiled from McQuarrie et al. (2008), Powers et al. (1998), Chirouze et al., (2013), Mugnier et al., (1999), Ojha et al., (2009), and T.P. Ojha (2012, personal commun.).

GEOLOGY, March 2014; v. 42; no. 3; p. 247–250; Data Repository item 2014089 | doi:10.1130/G35057.1 | Published online 10 January 2014

Similarly, detrital thermochronology of Siwalik sediments has dated the onset of exhumation of the frontal Siwaliks along the MFT to ca. 2 Ma in western and central Nepal (van der Beek et al., 2006) and ca. 1 Ma in Arunachal Pradesh (Chirouze et al., 2013), respectively.

Central to eastern Bhutan is the only segment of the Himalaya characterized by active structures in the foreland crust. There, the reverse faults bounding the Shillong Plateau have accommodated part of the convergence since ca. 9 Ma (Biswas et al., 2007; Clark and Bilham, 2008), i.e., before the onset of shortening of the FTB. Furthermore, contraction rates across the Bhutan Himalaya are no lower than those across other segments and follow the general west-to-east gradient of GPS velocities (Burgess et al., 2012). Accordingly, we conclude that the deformation trend within the Himalayan FTB is independent of shortening across the Shillong Plateau.

The two principal drivers of the Himalayan FTB appear to have remained constant since long before the onset of deformation. For example, convergence rates between the Indian and Eurasian plates have been steady since ca. 11 Ma (Molnar and Stock, 2009). Similarly, the Indian summer monsoon, which contributes most of the precipitation to the Himalaya, has been present since at least 12 Ma (Dettman et al., 2003). We suggest that the Himalayan FTB is in tectonic steady state because the physical characteristics of a wedge system approach steady values on a million-year time scale; in fact, the response time to any significant change in the parameters governing the morphology of the orogenic wedge is thought to be 0.25–2.5 m.y. (Whipple, 2009).

BALANCED CROSS SECTIONS

Several researchers have constructed balanced sections across the Himalayan FTB and have calculated shortening amounts and velocities (e.g., Schelling, 1992; Mugnier et al., 1999, 2004; Powers et al., 1998). However, establishing deformational and morphological trends along the Himalayan FTB using published data can be problematic owing to variations in the methods adopted to construct and balance cross sections and to revision of some of the parameters (e.g., timing of deformation) since their publication. To obtain an internally consistent data set that describes shortening of the Himalayan FTB, we compiled published and unpublished structural data to reconstruct eight published sections using Move 2D (www.mve.com/software/2dmove) (Fig. 2; Figs. DR3–DR6 in the GSA Data Repository[1]). Moreover, we constructed two new sections in eastern Bhutan and western Arunachal Pradesh (India) (red I and J in Fig. 1). We adopted the upper boundary of the Lower Siwalik subgroup as a common reference level to calculate shortening because it is the lowest and most complete formation; thus, it has accumulated the most strain within the Siwalik Group. We followed Mugnier et al. (2004), assuming that deformation within the Himalayan FTB commenced at the boundary between the Upper and Middle Siwalik; however, we verified and revised (where required) deformation age at each section using local stratigraphic ages for this boundary (Table 1).

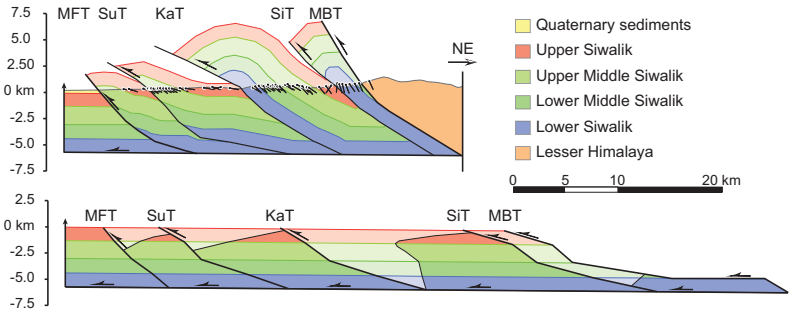

Figure 2. Illustrative cross section G from Figure 1. Top: Current geometry of wedge. Bottom: Retro-deformed wedge. MBT—Main Boundary thrust; SuT—Sunjhari thrust; KaT—Kamala thrust; SiT—Sindhuli thrust; MFT—Main Frontal thrust.

Results vary widely among the ten cross sections. Total shortening and shortening velocity are 8.3–37.7 km and 3.20–9.66 mm yr^{-1}, respectively, and exhibit no clear spatial pattern (Fig. 3A). In contrast, extension is remarkably constant (Table 1), with a mean of 0.48 ± 0.04 when the two westernmost sections are excluded. Strain rates increase steadily from west to east (2.52–6.96 × 10^{-15} s^{-1}; Fig. 3A) and are of the same order of magnitude as current strain rates (Fig. 3A; Kreemer et al., 2003). Moreover, the width of the FTB is highly variable, although it generally decreases from west to east (Fig. 3B).

DISCUSSION

Three principal processes govern the morphology of a critical Coulomb wedge (e.g., Dahlen et al., 1984): (1) growth in its mechanically critical state according to the mechanical properties of the rocks within the wedge; (2) accretion of material at a rate equal to the product of the convergence velocity and the thickness of the material; and (3) removal of material by erosion. Because the lithology of the Himalayan FTB is

TABLE 1. RESULTS FROM THE BALANCED AND RETRO-DEFORMED CROSS SECTIONS

Section	Shortening (km)	Extension $e = \Delta L/L_0$	Age of Upper/Middle Siwalik boundary, t (Ma)	Shortening velocity (mm yr^{-1})	Strain rate $\dot{e} = e/t$ (s^{-1})	Sediment thickness (m)	Sediment accreted volume flux (m^2 yr^{-1})
A	23.0 ± 3.47	0.22	2.70 ± 0.3	8.52 ± 1.60	2.52 × 10^{-15} ± 4.73 × 10^{-16}	7546	64.3 ± 12.1
B	10.6 ± 2.67	0.23	2.70 ± 0.3	3.93 ± 1.08	2.75 × 10^{-15} ± 7.56 × 10^{-16}	–	–
C	25.7 ± 2.21	0.41	4.83 ± 1.0	5.32 ± 1.19	2.70 × 10^{-15} ± 6.05 × 10^{-16}	6472	34.4 ± 7.7
D	37.7 ± 8.77	0.49	4.83 ± 1.0	7.81 ± 2.43	3.20 × 10^{-15} ± 9.97 × 10^{-16}	6376	49.8 ± 15.5
E	31.1 ± 3.22	0.48	3.22 ± 0.3	9.66 ± 1.35	4.74 × 10^{-15} ± 6.61 × 10^{-16}	5091	49.2 ± 6.9
F	27.0 ± 2.98	0.46	3.22 ± 0.3	8.39 ± 1.21	4.54 × 10^{-15} ± 6.55 × 10^{-16}	5286	44.3 ± 6.4
G	29.3 ± 1.52	0.44	3.42 ± 0.6	8.57 ± 1.57	4.03 × 10^{-15} ± 7.37 × 10^{-16}	5733	49.1 ± 9.0
H	32.6 ± 2.29	0.48	3.42 ± 0.6	9.53 ± 1.80	4.46 × 10^{-15} ± 8.42 × 10^{-16}	5340	50.9 ± 9.6
I	8.31 ± 1.45	0.57	2.60 ± 0.3	3.20 ± 0.67	6.96 × 10^{-15} ± 1.46 × 10^{-16}	2931	9.4 ± 2.0
J	16.5 ± 1.91	0.44	2.60 ± 0.3	6.35 ± 1.04	5.40 × 10^{-15} ± 8.82 × 10^{-16}	4736	44.8 ± 7.3

Note: See Figure 1 for section locations. Errors in the cross sections were determined using the area-balancing error method (Judge and Allmendinger, 2011). The 1σ uncertainties were propagated from the errors in the cross sections and uncertainties on stratigraphic ages (see text). We use the standard definition of the linear strain, extension, as the ratio of change of length (ΔL) and the initial length (L_0). The deformation age at each section was determined using the local stratigraphic age of the Upper/Middle Siwalik Group boundary (Fig. DR1 [see text footnote 1]).

[1]GSA Data Repository item 2014089, Figures DR1–DR7 (magnetostratigraphic correlation of the Siwalik Group across the Himalayan arc, detailed geological maps, balanced and retro-deformed section, location of swaths used to calculate rainfall and the specific steam power), is available online at www.geosociety.org/pubs/ft2014.htm, or on request from editing@geosociety.org or Documents Secretary, GSA, P.O. Box 9140, Boulder, CO 80301, USA.

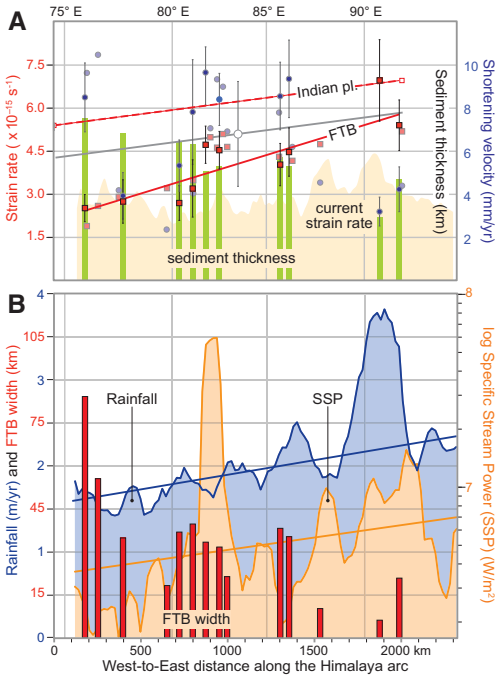

Figure 3. A: Graph of shortening velocity (blue circles), strain rate (red squares), and sediment thickness (green bars) of Siwalik Group plotted against distance along Himalayan arc. Dark and pale colors represent data from this study and published sections, respectively. Red line is best fit of strain rate in Himalayan fold-and-thrust belt (FTB). Plate strain rate (dashed red line) was calculated from plate convergence velocity of Molnar and Stock (2009), assuming Indian plate motion is distributed over lithosphere with thickness of 200 km. Gray circle is average shortening velocity and gray line is shortening velocity scaled to vary at same rate as plate convergence velocity. B: Graph plotting width of Himalayan FTB with distance along Himalayan arc against total annual rainfall and specific steam power (SSP). The oscillations in SSP along strike are associated with variations in rainfall (discharge), catchment size, and channel slope distribution within the catchment.

homogeneous, potential along-strike variations in wedge deformation and morphology can be explained by accretionary and erosional fluxes that are locally steady but vary along strike.

Accretion of Material

Convergence in a critical Coulomb wedge is accommodated by (1) material flux from the back of the orogenic wedge, (2) accretion of material from the foreland, and (3) sliding of the wedge over the foreland. Owing to the lack of data constraining the flux of material from the back of the belt, we considered an end member in which erosion of mass from north of the MBT is sufficient to prevent any introduction of material into the Himalayan FTB from the north.

The spatial distribution of strain rates calculated from the cross sections correlates well with that of strain rates associated with Indian plate convergence (Fig. 3A). Convergence velocities between the Indian and Eurasian plates have been shown to vary laterally from ~34 mm yr^{-1} in the northwest to ~44 mm yr^{-1} in the northeast of India (Molnar and Stock, 2009). This trend is reflected in the current contraction rates across the Himalaya, which are ~15 mm yr^{-1} greater in the east than the west (Burgess et al., 2012). In contrast, long-term shortening velocities exhibit no spatial trend, which impedes calculation of material flux into the Himalayan FTB. The variable amount of shortening registered in Himalayan molasse may be caused by the foreland sedimentary basin geometry, which is complicated by sediment transport characteristics and the geometry of sub-basins (Burbank et al., 1996).

Comparison of Holocene slip rates across the MFT (i.e., ~21–23.4 mm yr^{-1}; Lavé and Avouac, 2000; Burgess et al., 2012; Mugnier et al., 2004) with the long-term shortening velocities suggests that only a third to half of the Neogene molasse was accreted to the Himalayan FTB. Actually, field observations (Husson et al., 2004; Mugnier et al., 1999) suggest that part of the molasse descends beneath the backstop. Thermal kinematic models of the Himalaya (e.g., Herman et al., 2010) have demonstrated that the convergence is partitioned into overthrusting and underthrusting with a partitioning factor λ of ~0.7, indicating that about a third of the convergence is accommodated by overthrusting at rates of 6–7 mm yr^{-1}. This is consistent with our observations.

The average velocity of 6.8 ± 2.4 mm yr^{-1} multiplied by the measured sediment thickness within the FTB yields an eastward decrease in material flux. Because plate convergence velocities were 13% higher in the east than the west during the deformation of the Himalayan molasse, scaling the average shortening velocity arbitrarily to obtain an equivalent velocity trend along the FTB yields a laterally constant mass accretion rate (represented by cross-sectional volumetric flux) of ~40–60 m^2 yr^{-1} (Table 1), equivalent to the estimate by Husson et al. (2004). Although the values we have calculated may be subject to larger uncertainties, we are confident that the lateral trends obtained correspond to those present in the field.

Wedge Erosion

Surface mass transport on the Himalayan FTB is controlled by the Indian summer monsoon (Bookhagen and Burbank, 2010). Rainfall and associated runoff are primary drivers of erosional mass removal from a wedge, the rate, ε, of which is often described by a bedrock incision law and has been argued to be controlled by a stream-power erosion law described by channel slope (S), catchment area (A, a proxy for discharge), and erosional efficiency (K): $\varepsilon = -KA^m S^n$, where m and n are power law exponents (Whipple and Tucker, 1999). The erodibility factor K is a dimensional coefficient of erosion that incorporates the effects of changes in river channel geometry, effective precipitation, and the resistance of bedrock to fluvial incision. Higher values of K, corresponding to more efficient erosion, have been shown to favor a narrower wedge (Whipple, 2009). The Siwalik Group lithologies are homogeneous throughout the Himalayan FTB (Burbank et al., 1996), resulting in constant rock erodibility along strike and leaving climate as the primary parameter controlling the erodibility factor K.

To characterize along-strike climatic variation, we extracted annual rainfall amounts and specific stream power (SSP), calculating the median rainfall and the sum of SSP over the Himalayan FTB (Fig. DR7). SSP was calculated according to Bookhagen and Strecker (2012). In short, SSP is the product of the specific weight of water, discharge (adopted from calibrated remote-sensing rainfall data; cf. Bookhagen and Burbank, 2010), and channel slope divided by channel width. SSP is a proxy for fluvial erosion, although it relies on discharge calculated from calibrated remote-sensing rainfall data; thus, it more accurately reflects climatic impacts in areas with steep rainfall gradients. A distinct eastward-increasing gradient in rainfall rates and in SSP can be seen in the Himalayan FTB, concomitant with the eastward decrease of belt width (Fig. 3B).

Interplay of Convergence Velocity and Climate

Analytical coupled erosion-deformation models (e.g., Hilley and Strecker, 2004) have demonstrated that the morphology of a steady-state wedge at its Coulomb failure limit is controlled by (1) the mechanical properties of rocks in the wedge, (2) the décollement sole-out depth, (3) erosional exponents, (4) basin hydrological parameters, and (5) the ratio of the flux of the tectonically added material to the erodibility factor (hV/K). The first three parameters remain almost constant along the Himalayan FTB, whereas along-strike variations in hydrological parameters were addressed in the previous section. Similarly, all of the components of the last parameter are known to vary laterally. In general, increasing hV/K produces wider wedges (Hilley and Strecker, 2004; Whipple, 2009). Increases in this ratio may result from increasing material flux (hV) introduced into the wedge, or decreased erosional power due to reduced precipitation and runoff (discharge), here exemplified by SSP.

Poorly constrained long-term shortening velocities preclude accurate and precise calculation of the material flux. Circumstantial evidence suggests that the material flux either slightly decreases eastward or remains approximately constant along the arc. Assuming the latter, which is more likely, the steady-state wedge width equation,

$$W = \frac{hV}{\dot{e}} \approx \frac{1}{\dot{e}},$$

indicates that wedge width is inversely proportional to erosion rate. In summary, the observed eastward decrease of the Himalayan FTB width is consistent with the eastward increase of precipitation and the SSP on the Himalayan foothills.

CONCLUSIONS

Within the active foreland fold-and-thrust belt of the Himalaya, extension, strain rate, and belt morphology vary systematically from west to east. Strain rates correlate well with west-to-east increases in convergence rates according to both long-term plate velocity data and GPS data, suggesting that Pliocene to Holocene shortening is externally imposed and related to plate convergence rates. Conversely, the eastward decrease in belt width corresponds to an eastward increase in rainfall rates and specific stream power. Although mass accretion rates have not been well constrained, we argue that they remain relatively constant along the FTB.

We suggest that the morphology of the Himalayan FTB is controlled primarily by erosion, in accordance with the critical taper model. Surface-material removal is mainly controlled through rainfall and runoff and can be expressed as specific stream power. Of the parameters considered, lithology, erodibility, and rock mechanical properties are relatively homogeneous throughout the belt. Thus, we conclude that climatically induced erosion is the principal control on Himalayan foreland fold-and-thrust belt morphology.

ACKNOWLEDGMENTS

We thank G. Hilley and two anonymous reviewers for their constructive comments. Fieldwork in Bhutan was enabled by the invaluable help provided by the Royal Government of Bhutan (especially by Hon. Jigme Yoser Thinley), and by the Hoch family. The study was supported by the Natural Sciences and Engineering Research Council of Canada (NSERC, grant RGPIN/2274752009) and a grant by the National Geographic Society's Committee for Research and Exploration.

REFERENCES CITED

Avouac, J.P., 2003, Mountain building, erosion, and the seismic cycle in the Nepal Himalaya: Advances in Geophysics, v. 46, p. 1–80, doi:10.1016/S0065-2687(03)46001-9.

Beaumont, C., Fullsack, P., and Hamilton, J., 1992, Erosional control of active compressional orogens, *in* McClay, K.R., ed., Thrust tectonics: New York, Chapman and Hall, p. 1–18.

Biswas, S., Coutand, I., Grujic, D., Hager, C., Stöckli, D., and Grasemann, B., 2007, Exhumation and uplift of the Shillong plateau and its influence on the eastern Himalayas: New constraints from apatite and zircon (U-Th-[Sm])/He and apatite fission track analyses: Tectonics, v. 26, TC6013, doi:10.1029/2007TC002125.

Bookhagen, B., and Burbank, D.W., 2010, Toward a complete Himalayan hydrological budget: Spatiotemporal distribution of snowmelt and rainfall and their impact on river discharge: Journal of Geophysical Research, v. 115, F03019, doi:10.1029/2009JF001426.

Bookhagen, B., and Strecker, M.R., 2012, Spatiotemporal trends in erosion rates across a pronounced rainfall gradient: Examples from the southern Central Andes: Earth and Planetary Science Letters, v. 327–328, p. 97–110, doi:10.1016/j.epsl.2012.02.005.

Burbank, D., Beck, R.A., and Mulder, T., 1996, The Himalayan foreland basin, *in* Yin, A., and Harrison, T. M., eds., The tectonic evolution of Asia: Cambridge, UK, Cambridge University Press, p. 149–188.

Burgess, W.P., Yin, A., Dubey, C.S., Shen, Z.-K., and Kelty, T.K., 2012, Holocene shortening across the Main Frontal Thrust zone in the eastern Himalaya: Earth and Planetary Science Letters, v. 357, p. 152–167, doi:10.1016/j.epsl.2012.09.040.

Chirouze, F., Huyghe, P., van der Beek, P., Chauvel, C., Chakraborty, T., Dupont-Nivet, G., and Bernet, M., 2013, Tectonics, exhumation, and drainage evolution of the eastern Himalaya since 13 Ma from detrital geochemistry and thermochronology, Kameng River Section, Arunachal Pradesh: Geological Society of America Bulletin, v. 125, p. 523–538, doi:10.1130/B30697.1.

Clark, M., and Bilham, R., 2008, Miocene rise of the Shillong Plateau and the beginning of the end for the Eastern Himalaya: Earth and Planetary Science Letters, v. 269, p. 337–351, doi:10.1016/j.epsl.2008.01.045.

Dahlen, F.A., 1990, Critical taper model of fold-and-thrust belts and accretionary wedges: Annual Review of Earth and Planetary Sciences, v. 18, p. 55–99, doi:10.1146/annurev.ea.18.050190.000415.

Dahlen, F.A., Suppe, J., and Davis, D., 1984, Mechanics of fold-and-thrust belts and accretionary wedges: Cohesive Coulomb theory: Journal of Geophysical Research, v. 89, p. 10,087–10,101, doi:10.1029/JB089iB12p10087.

Dettman, D., Fang, X., Garzione, C., and Li, J., 2003, Uplift-driven climate change at 12 Ma: A long $\delta^{18}O$ record from the NE margin of the Tibetan plateau: Earth and Planetary Science Letters, v. 214, p. 267–277, doi:10.1016/S0012-821X(03)00383-2.

Herman, F., Copeland, P., Avouac, J., Bollinger, L., Mahéo, G., Le Fort, P., Rai, S., Foster, D., Pécher, A., Stüwe, K., and Henry, P., 2010, Exhumation, crustal deformation, and thermal structure of the Nepal Himalaya derived from the inversion of thermochronological and thermobarometric data and modelling of the topography: Journal of Geophysical Research, v. 115, B06407, doi:10.1029/2008JB006126.

Hilley, G., and Strecker, M., 2004, Steady state erosion of critical Coulomb wedges with applications to Taiwan and the Himalaya: Journal of Geophysical Research, v. 109, B01411, doi:10.1029/2002JB002284.

Hodges, K.V., 2000, Tectonics of the Himalaya and southern Tibet from two perspectives: Geological Society of America Bulletin, v. 112, p. 324–350, doi:10.1130/0016-7606(2000)112<324:TOTHAS>2.0.CO;2.

Husson, L., Mugnier, J.-L., Leturmy, P., and Vidal, G., 2004. Kinematics and sedimentary balance of the Sub-Himalayan zone, western Nepal, *in* McClay, K.R., ed., Thrust tectonics and hydrocarbon systems: American Association of Petroleum Geologists Memoir 82, p. 115–130.

Judge, P.A., and Allmendinger, R.W., 2011, Assessing uncertainties in balanced cross sections: Journal of Structural Geology, v. 33, p. 458–467, doi:10.1016/j.jsg.2011.01.006.

Kreemer, C., Holt, W.E., and Haines, A.J., 2003, An integrated global model of present-day plate motions and plate boundary deformation: Geophysical Journal International, v. 154, p. 8–34, doi:10.1046/j.1365-246X.2003.01917.x.

Lavé, J., and Avouac, J., 2000, Active folding of fluvial terraces across the Siwaliks Hills, Himalayas of central Nepal: Journal of Geophysical Research, v. 105, p. 5735–5770, doi:10.1029/1999JB900292.

McQuarrie, N., Robinson, D., Long, S., Tobgay, T., Grujic, D., Gehrels, G., and Ducea, M., 2008, Preliminary stratigraphic and structural architecture of Bhutan: Implications for the along strike architecture of the Himalayan system: Earth and Planetary Science Letters, v. 272, p. 105–117, doi:10.1016/j.epsl.2008.04.030.

Molnar, P., and Stock, J.M., 2009, Slowing of India's convergence with Eurasia since 20 Ma and its implications for Tibetan mantle dynamics: Tectonics, v. 28, TC3001, doi:10.1029/2008TC002271.

Mugnier, J., Leturmy, P., Huyghe, P., Chalaron, E., Vidal, G., Husson, L., and Delcaillau, B., 1999, The Siwaliks of western Nepal: I. Geometry and kinematics: Journal of Asian Earth Sciences, v. 17, p. 629–642, doi:10.1016/S1367-9120(99)00038-3.

Mugnier, J.L., Huyghe, P., Leturmy, P., and Jouanne, F., 2004, Episodicity and rates of thrust sheet motion in Himalaya (western Nepal), *in* McClay, K.R., ed., Thrust tectonics and hydrocarbon systems: American Association of Petroleum Geologists Memoir 82, p. 91–114.

Ojha, T.P., Butler, R.F., DeCelles, P.G., and Quade, J., 2009, Magnetic polarity stratigraphy of the Neogene foreland basin deposits of Nepal: Basin Research, v. 21, p. 61–90, doi:10.1111/j.1365-2117.2008.00374.x.

Powers, P.M., Lillie, R.J., and Yeats, R.S., 1998, Structure and shortening of the Kangra and Dehra Dun reentrants, sub-Himalaya, India: Geological Society of America Bulletin, v. 110, p. 1010–1027, doi:10.1130/0016-7606(1998)110<1010:SASOTK>2.3.CO;2.

Schelling, D., 1992, The tectonostratigraphy and structure of the eastern Nepal Himalaya: Tectonics, v. 11, p. 925–943, doi:10.1029/92TC00213.

van der Beek, P., Robert, X., Mugnier, J.-L., Bernet, M., Huyghe, P., and Labrin, E., 2006, Late Miocene–Recent exhumation of the central Himalaya and recycling in the foreland basin assessed by apatite fission-track thermochronology of Siwalik sediments, Nepal: Basin Research, v. 18, p. 413–434, doi:10.1111/j.1365-2117.2006.00305.x.

Whipple, K.X, 2009, The influence of climate on the tectonic evolution of mountain belts: Nature Geoscience, v. 2, p. 97–104, doi:10.1038/ngeo413.

Whipple, K.X, and Tucker, G.E., 1999, Dynamics of the stream-power river incision model: Implications for height limits of mountain ranges, landscape response timescales, and research needs: Journal of Geophysical Research, v. 104, p. 17,661–17,674, doi:10.1029/1999JB900120.

Willett, S., Beaumont, C., and Fullsac, P., 1993, Mechanical model for the tectonics of doubly vergent compressional orogens: Geology, v. 21, p. 371–374, doi:10.1130/0091-7613(1993)021<0371:MMFTTO>2.3.CO;2.

Manuscript received 23 August 2013
Revised manuscript received 4 December 2013
Manuscript accepted 11 December 2013

Printed in USA